How to cite:
International Edition: doi.org/10.1002/anie.201915074
German Editon: doi.org/10.1002/ange.201915074

Charge Transfer at Interfaces

Insights into Charge Transfer at an Atomically Precise Nanocluster/Semiconductor Interface

Yu Wang[+], Xiao-He Liu[+], Qiankun Wang, Martin Quick, Sergey A. Kovalenko, Qing-Yun Chen,* Norbert Koch, and Nicola Pinna**

Abstract: *The deposition of an atomically precise nanocluster, for example, $Ag_{44}(SR)_{30}$, onto a large-band-gap semiconductor such as TiO_2 allows a clear interface to be obtained to study charge transfer at the interface. Changing the light source from visible light to simulated sunlight led to a three orders of magnitude enhancement in the photocatalytic H_2 generation, with the H_2 production rate reaching 7.4 $mmol\,h^{-1}\,g_{catalyst}^{-1}$. This is five times higher than that of TiO_2 modified with Ag nanoparticles and even comparable to that of TiO_2 modified with Pt nanoparticles under similar conditions. Energy band alignment and transient absorption spectroscopy reveal that the role of the metal clusters is different from that of both organometallic complexes and plasmonic nanoparticles: A type II heterojunction charge-transfer route is achieved under UV/Vis irradiation, with the cluster serving as a small-band-gap semiconductor. This results in the clusters acting as co-catalysts rather than merely photosensitizers.*

Ligand-protected metal nanoclusters (NCs) have shown great potentials in the field of energy conversion, as their electronic structures can be precisely tuned by varying their size (i.e. number of metal atoms), composition, and nanostructure.[1–5] Current studies on the utilization and conversion of light energy focus on the sensitization ability of metal NCs and aim to exploit the part of the solar spectrum that large band-gap semiconductors (i.e. TiO_2, ZnO) are not capable of.[6–10] The energy absorbed from visible photons is temporarily stored within the NCs before being released or transferred into the semiconductor.[11–14] By varying the atomic packing of gold NCs, the lifetime of the excited state can be as long as 5 μs, which is comparable to bulk silicon.[15] Extending the photoresponse of semiconductors from the UV to the Vis/IR region enables visible-light-driven photocatalytic and photoelectrochemical reactions, such as hydrogen generation and CO_2 reduction.[16–22] Despite advances in research, the role of NCs in hybrid materials is still in the early stages compared to organometallic dyes.[23] Considering that metal NCs with distinct gaps between the highest occupied molecular orbital (HOMO) and the lowest unoccupied molecular orbital (LUMO) can produce excitons (electron–hole pairs) after absorbing light, it is reasonable to treat them as small-band-gap semiconductors.[24–26] Under simulated sunlight, both the NCs and the semiconductor will be excited. Then, comes an essential question: Does the combination of metal NCs with a large-band-gap semiconductor show a synergistic effect on light harvesting and charge separation at the binary semiconductor heterojunction, as is evident with the natural photosynthesis system? Addressing this question could also lead to practical applications, as sunlight is the most abundant and also free renewable energy resource.

Plasmonic metal nanoparticles (NPs) represent another kind of sensitization materials which could extend the photoresponse to longer wavelengths.[27–29] The position of the surface plasmonic resonance (SPR) peak can be tuned by controlling the shape and size of the NPs.[29] Noble metals (e.g. Pt) with a high work function can readily extract the excited electrons from the semiconductor through the Schottky junction and use these electrons to reduce the protons adsorbed on their surface, thereby resulting in an enhanced photocatalytic performance.[30,31] However, NPs with a certain shape and size only harvest the photon energy in a narrow range within the visible and infrared region.[29] To improve the utilization of sunlight, NPs with different sizes need to be integrated, but this results in complications in the system. Moreover, the size of the NPs affects their ability to extract electrons from the semiconductor.[32–34] The smaller the size of the NPs, the higher the energy level of the NPs.[32] Once the energy levels of the NPs become higher than the conduction band (CB) of the semiconductor, the NPs will lose their ability to extract electrons.[33] Once the NPs reach a critical size, they will capture both electrons and holes, thereby acting

[*] Dr. Y. Wang,[+] Dr. M. Quick, Dr. S. A. Kovalenko, Prof. N. Pinna
Institut für Chemie and IRIS Adlershof
Humboldt-Universität zu Berlin
Brook-Taylor-Strasse 2, 12489 Berlin (Germany)
E-mail: wangyuxx@hu-berlin.de
nicola.pinna@hu-berlin.de
Dr. Q. Wang, Prof. N. Koch
Institut für Physik and IRIS Adlershof
Humboldt-Universität zu Berlin
Brook-Taylor-Strasse 6, 12489 Berlin (Germany)
X.-H. Liu,[+] Prof. Q.-Y. Chen
International Research Center for Renewable Energy (IRCRE) and State Key Laboratory of Multiphase Flow in Power Engineering
School of Energy and Power Engineering
Xi'an Jiaotong University
Xi'an 710049 (P. R. China)
E-mail: qychen@mail.xjtu.edu.cn
[+] These authors contributed equally to this work.
Supporting information and the ORCID identification number for some of the authors of this article can be found under: https://doi.org/10.1002/anie.201915074.

as a recombination center.[34] Furthermore, the larger the particle size, the smaller the specific area, which leads to a lower exposure to the active center.[2] The discrete energy levels of metal NCs endow them with multiple absorptions within the UV/Vis/IR region.[14] Moreover, they have already proven to be catalytically active.[35–39] This provides an opportunity in photocatalytic systems for the metal NCs to serve as both the light absorber and co-catalyst.

With these motivations, we deposited atomically precise silver NCs $Ag_{44}(SR)_{30}$ (denoted as **1**, SR = thiolate) on the large-band-gap metal oxide semiconductor TiO_2 and studied the photocatalytic H_2 production performance. By changing the excitation energy from only the visible to the full solar spectrum, the charge-transfer pathway of the system can be readily tuned to a type II photocatalysis mechanism. In addition to the extension of the photoresponse, the synergistic effect between the NCs and TiO_2 was found to contribute significantly to the enhanced catalytic performance. Thus, the bifunctional role of NCs as the light absorber and co-catalyst for photocatalytic H_2 production was revealed.

The synthesis of **1** is described in the Experimental Section. Five apparent absorption bands at $\lambda = 412$, 483, 535, 641, and 833 nm are observed (Figure 1a).[40] The high molar extinction coefficient (ε) of **1** indicates its good light-harvesting ability (Figure S1).[14] For example, the ε value for the absorption at $\lambda = 483$ nm is $1.1 \times 10^5\ cm^{-1}M^{-1}$, four times higher than that of commonly employed gold NCs.[41] It should be noted that previous studies show that the HOMO–LUMO gap of **1** (0.77 eV) is smaller than the optical band gap, because the electron transition from the HOMO to the LUMO (superatom 1D to 2S) is optically forbidden.[40,42,43] The electrospray ionization (ESI) mass spectrum (see Figure S3) of **1** showed a peak at m/z 2274.2, and its isotopic patterns were in perfect agreement with the simulated pattern, thus indicating **1** carries four negative charges (Figure S4).[40] Figure 1b shows the UV/Vis spectra of the TiO_2 film before and after the deposition of **1**. The enhanced absorption of **1**-TiO_2 in the visible region is attributed to **1**. Multiple bands at $\lambda = 380$, 500, and 600 nm, rather than an SPR absorption band of Ag NPs, indicate that the NCs maintain their size after deposition onto a TiO_2 film.[40]

To assess the solid-state properties of the cluster/TiO_2 composite, the energy band alignment of **1**-TiO_2 was measured with ultraviolet photoelectron spectroscopy (UPS), which is a helpful way to study whether metal NCs with distinct energy gaps can be treated as small-band-gap semiconductors. The secondary electron cutoffs (SECOs) were measured to be 3.9 eV and 4.7 eV before and after deposition of the clusters, respectively. This indicates an increase in the work function ($\Delta\varphi$) of 0.8 eV (Figure 1c). The Ti $2p_{3/2}$ core level band shifts to a lower binding energy upon deposition, thus pointing to an upward bending of the band ($\Delta\varphi_{BB}$ of 0.7 eV (Figure 1d). Thus, the contribution to the change in the work function from the formation of an interface dipole ($\Delta\varphi_{ID}$) is small (0.1 eV).[44] From the UPS spectra (Figure 1e), the valence band maximum (E_{VBM}) of TiO_2 was found to be located at 3.2 eV (below the Fermi level, E_F). The HOMO of **1** was measured to be at 0.7 eV (Figure S5). Application of the equation $E_{LUMO} = E_{HOMO\text{–}LUMO\,gap} - E_{HOMO}$ therefore computes the LUMO of **1** to be 0.07 eV above E_F.[40]

Figure 2a shows the energy level diagram of the cluster/TiO_2 system deduced from the above results. The contact of **1** to TiO_2 leads to bending of the TiO_2 surface band and thus a change in the near-surface space-charge region. Electrons in

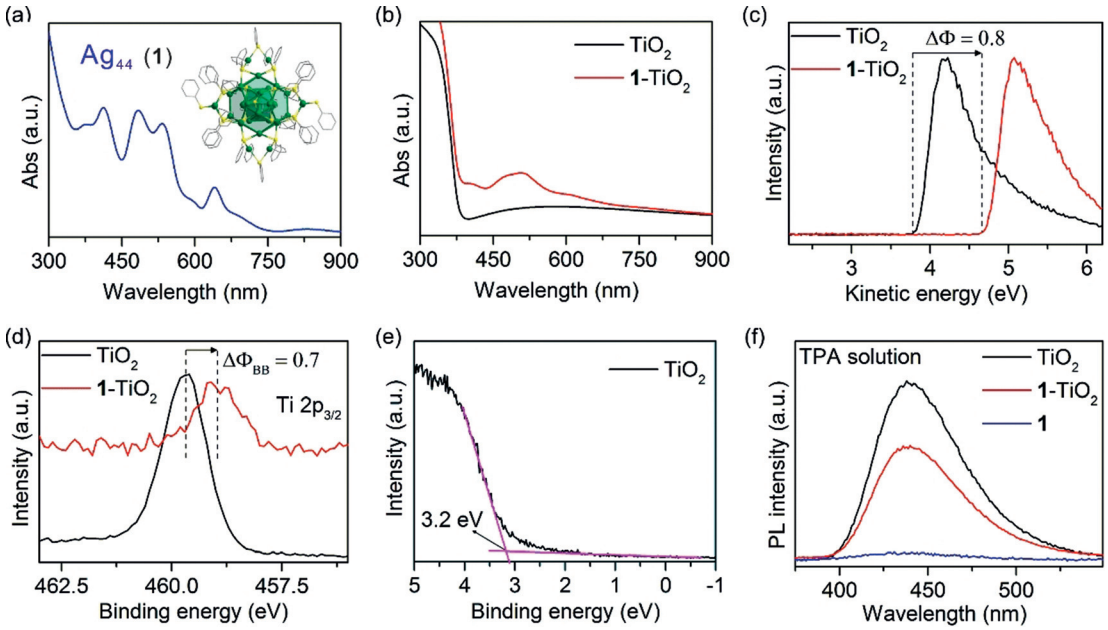

Figure 1. a) UV/Vis absorption spectrum of Ag_{44} NCs (**1**) in solution. b) UV/Vis absorption spectrum of the TiO_2 film before and after deposition of **1**. c) Secondary electron cutoff for the TiO_2 film before (black) and after (red) deposition of **1**. d) The shift of Ti $2p_{3/2}$ after the deposition of **1**. e) Valence band XPS spectrum of pristine TiO_2 film. f) Fluorescence spectra of TiO_2 film (black), **1**-TiO_2 (red), and **1** (blue) in terephthalate solution irradiated by UV/Vis light.

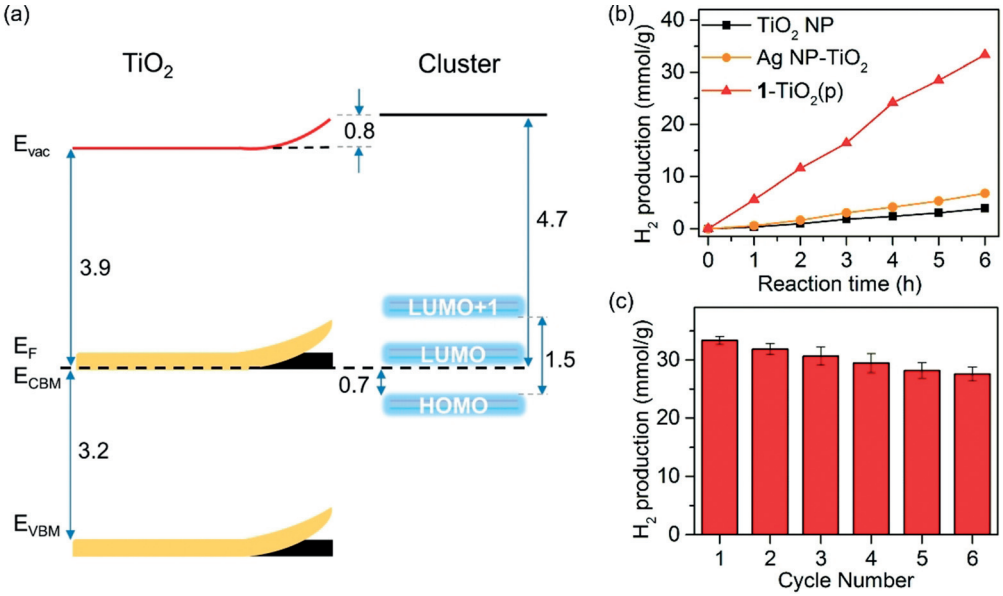

Figure 2. a) Schematic energy level diagram of TiO_2 before (black) and after (orange) deposition of the NCs. All numbers are given in eV. b) Catalytic hydrogen evolution by photocatalysts under UV/Vis light (100 $mW cm^{-2}$). TiO_2 NPs: black, TiO_2 NPs modified with Ag NPs: orange, and **1**-TiO_2(p) NPs: red. c) Cycling test over **1**-TiO_2(p) NPs under UV/Vis light (100 $mW cm^{-2}$).

TiO_2 will transfer to **1** until their Fermi levels are electrically aligned. Consequently, the formation of an internal built-in electric field is beneficial for the separation and transport of carriers. The interaction between **1** and TiO_2 alters the energy levels of **1**, which accounts for the broadening of the bands of **1**-TiO_2 in the visible region, compared with pure **1** (Figure S6).[45] When both TiO_2 and **1** are excited, the photoinduced holes in the valence band of TiO_2 will be readily transferred to the HOMO of **1**, thereby separating them from the photoinduced electrons. This is similar to the scenario in a straddling semiconductor heterojunction.[46,47] Note that the observed absorption band of **1** at $\lambda = 833$ nm is attributed to electron promotion from the HOMO to LUMO + 1.[40] Thus, the position of LUMO + 1 is calculated to be 0.8 eV above the E_F, which is higher than the conduction band minimum (CBM) of TiO_2.[40] Therefore, it is expected that when electrons in **1** are photoexcited to LUMO + m ($m \geq 1$) levels, electron–hole separation is processed through a staggered type II pathway. In this case, electrons in **1** will transfer to the CB of TiO_2 and, simultaneously, holes at TiO_2 will inject into the HOMO of **1**. This process can reduce the resistance to charge transfer and improve the efficiency of the charge separation, which will further result in an improved photocatalytic performance.[47]

The distribution of holes under UV/Vis irradiation was studied by probe experiments. Nonfluorescent terephthalate (TPA) was used as a probe for detecting the formation of hydroxyl radicals, which are one of the products of water oxidation ($^{\bullet}OH/H_2O$, 2.3 V versus NHE).[48] For a solution of TPA with TiO_2, a photoluminescence (PL) band at $\lambda = 435$ nm appears and increases gradually as the illumination continues (Figure S7). As the edge of the TiO_2 valence band (VB) is more positive than the potential of $^{\bullet}OH/H_2O$, it can be deduced that, under irradiation, the holes in the VB of TiO_2 oxidize H_2O to $^{\bullet}OH$, which further reacts with TPA to produce highly fluorescent hydroxyterephthalate (HTPA).[48] The solution of TPA with clusters shows negligible PL after irradiation, in good agreement with the observations that the HOMO of **1** is less positive than the VB of TiO_2 (Figure 1 f). The solution of TPA with **1**-TiO_2 shows a much weaker PL band at $\lambda = 435$ nm compared to TiO_2. This supports the hypothesis that photoinduced holes in TiO_2 transfer to the HOMO of **1**.

To verify the superiority of the composite in photocatalytic reactions, the NCs were loaded on commercial TiO_2 NPs at a weight percentage of 2%. For distinction, the particulate **1**-TiO_2 photocatalyst is defined as **1**-TiO_2(p). The matrix-assisted laser desorption ionization (MALDI) mass spectrum of **1**-TiO_2(p) shows a broad signal around m/z 8900 (assigned to fragments of **1**), thus indicating the successful deposition of **1** on the TiO_2 NPs (Figure S8). The photocatalytic hydrogen evolution performance of the **1**-TiO_2(p) NPs was first examined under irradiation with visible light, with reference to the pure TiO_2 NPs (Figure S9). Whereas the latter shows no hydrogen production, the activity increases when **1** is coupled to the TiO_2 NPs, with 0.07 μmol H_2 detected after 1 h (see Figure S9). The H_2 production rate increases over the next three hours at an average rate of 8.4 $\mu mol\, h^{-1} g_{catalyst}^{-1}$. Considering the fact that no Pt NP co-catalysts are employed in this case, **1** seems to be a promising photosensitizer compared to the previously reported gold NCs.[18] Surprisingly, the **1**-TiO_2(p) NPs exhibit a three orders of magnitude enhancement of H_2 production when the light is switched from visible light to simulated sunlight with equivalent intensity (Figure 2 b). The rate of hydrogen production under simulated sunlight reaches an average of 5.5 $mmol\, h^{-1} g_{catalyst}^{-1}$ in 6 h, with a maximum of 7.4 $mmol\, h^{-1} g_{catalyst}^{-1}$. This performance is ten times higher than that of the pure TiO_2 NPs and five times higher than that of TiO_2 NPs modified with Ag NPs. The rate of hydrogen production by the **1**-TiO_2(p) photocatalytic system is, in fact, comparable to that of the TiO_2 NPs modified with Pt NPs under the same conditions (Figure S10). Such a large improvement in the photocatalytic performance can not be attributed solely to the photoresponse extension of the TiO_2 NPs alone. In addition, **1**-TiO_2(p) NPs exhibit good stability, with 83% of the photocatalytic activity remaining after five cycles (Figure 2 c). The Ag 3d XPS spectra of **1**-TiO_2(p) before and after the reaction show no apparent change (Fig-

ure S11).[49,50] Furthermore, no larger nanoclusters were observed in a wider range mass spectrometric analysis (e.g. from m/z 10000 up to 35000) after the reaction (Figure S8).

Since methanol serves as the sacrificial electron donor, carbon dioxide instead of molecular oxygen is detected as the oxidation product.[18] Besides methanol, other hole scavengers such as ethanol and ethylene glycol were employed, but **1**-TiO_2(p) exhibits its best performance when in an aqueous methanol solution (see Figure S12). This result is attributed to the easier oxidation of methanol, which captures the holes timely and thus suppresses the charge-recombination processes.[51]

Photoelectrochemical (PEC) measurements were further carried out to study the charge generation and separation processes. Figure 3a shows the transient photocurrent responses of **1**-TiO_2(p) under intermittent irradiation with UV and UV/Vis light. For comparison, the light intensity was fixed at 100 mw cm^{-2}. The higher photocurrent density under irradiation with UV/Vis light suggests a higher charge-separation efficiency.[52,53] An electrochemical impedance spectroscopy (EIS) study further supported this conclusion. As shown in Figure 3b, the Nyquist plot of **1**-TiO_2(p) under UV/Vis light exhibits a more depressed semicircle in the low-frequency region than under visible light, thus indicating that **1**-TiO_2(p) experiences a more efficient interfacial electron-transfer process under UV/Vis light.[20] This indicates that the charge transfer pathways under irradiation with visible and UV/Vis light are different. The smaller charge-transfer resistance of **1**-TiO_2(p) (Figure 3c), compared with the TiO_2 NPs, is consistent with the transient photocurrent response data (Figure S13) and the band alignment discussion above. A comparison of the Mott–Schottky plots for the pure TiO_2 NPs and **1**-TiO_2(p) are presented in Figure 3d. Both curves show a positive slope, thus indicating that the deposition of the NCs on the TiO_2 NPs does not change the n-type behavior of the TiO_2.[20] The flat band potential of TiO_2 NPs and **1**-TiO_2(p) are estimated to be −0.33 and −0.68 V versus Ag/AgCl, respectively. The cathodic shift of the flat band potential is consistent with the conclusion reached in the photoelectron spectroscopy study that the deposition of **1** results in an upward bending of the TiO_2 band. Figure 3e shows the PL spectra of the pure TiO_2 NPs and **1**-TiO_2(p). The band from TiO_2 at $\lambda = 430$ nm is almost quenched upon deposition of **1**, which suggests that the recombination of the photogenerated electron–hole pairs over **1**-TiO_2(p) is effectively suppressed.[54]

The increased light absorption in the UV region definitely contributes to the enhanced photocatalytic performance. The role of **1** in the charge separation should also be considered. To eliminate the influence of **1** absorbing light in the UV region, the absorbed photon to current efficiency (APCE) of **1**-TiO_2(p) and the pure TiO_2 NPs were compared (Figure 3f). The APCE at $\lambda = 300$, 310, 320, 330, and 340 nm are 10.9%, 8.9%, 8.4%, 8.1%, and 7.8%, for **1**-TiO_2 and 8.0%, 5.3%, 4.7%, 4.4%, and 3.9% for TiO_2. The higher APCE of **1**-TiO_2(p) indicates that it can convert the absorbed photons into current more efficiently, which agrees with the EIS and band alignment study results.[14]

To gain further insight into the electron dynamics of **1**-TiO_2 in real time, we relied on ultrafast transient absorption (TA) spectroscopy. Excitation at $\lambda = 380$ nm results in the creation of an electron–hole pair on the TiO_2 film within the pump-probe correlation time (Figure S14). The signal is weak, which is why recombination in the next 100 ps is concluded from the recovery of the bleaching upon excitation at $\lambda = 325$ nm (Figure S14).[54] It is assumed that excitation at

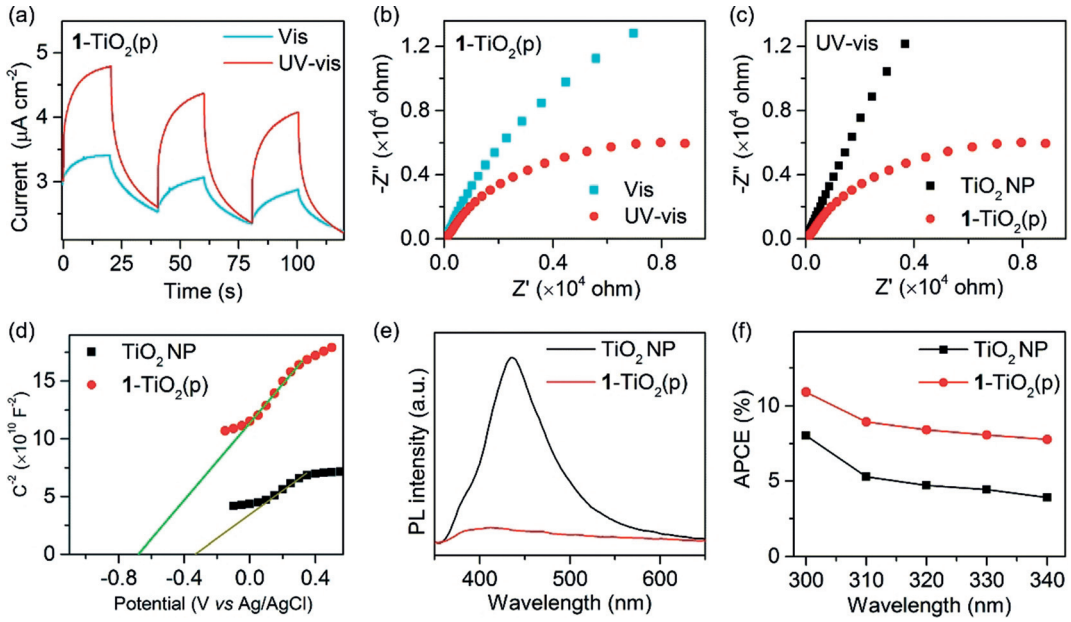

Figure 3. a) Transient photocurrent responses of **1**-TiO_2(p) NPs under UV/Vis and visible light. b) Nyquist phots of **1**-TiO_2(p) NPs under different light sources. c) Nyquist plots of TiO_2 NPs and **1**-TiO_2(p) NPs under UV/Vis light. The UV/Vis light and visible light have the same intensity of 100 mw cm^{-2}. d) Mott–Schottky plots of TiO_2 NPs and **1**-TiO_2(p) NPs in the dark. e) PL spectra of TiO_2 NPs before and after the deposition of **1**. f) Absorbed photon to current efficiency of pristine TiO_2 NPs and **1**-TiO_2(p) NPs in the UV region.

$\lambda_{exc} = 380$ nm results in higher excited states S_n of **1**-TiO_2 being initially populated, as evident by the difference in the extinction spectra of **1**-TiO_2 and TiO_2 (Figure S14).

The transient absorption spectra of **1**-TiO_2 are shown as 2D plots in Figures 4a,b and Figure S14. The kinetics can be summarized with the band integrals (BIs) from the data and the global kinetic analysis (Figures 4d,e). A positive signal is caused by excited-state absorption (ESA), and negative contributions indicate stimulated emission (SE) and bleaching. SE coincides with the $S_1 \leftarrow S_0$ transition and shows up within the pump-probe correlation time; thus indicating there is an ultrafast transition from S_n towards the S_1 state on the same fast time scale.

After pumping, early evolution of photoexcited **1**-TiO_2 is evident within the first 0.7 ps by partial decay of the ESA (Figure 4d, blue) accompanied by a decaying oscillation ($\nu = 2.5$ ps^{-1}, 85 cm^{-1}) visible between $\lambda = 414$ and 440 nm (Figure 4d, red). The oscillation frequency matches the acoustic phonons usually observed in moderately sized clusters.[55] Subsequently, with a time constant of 2.4 ps, the SE band vanishes and gives rise to residual or new ESA. Previously, such behavior was interpreted as electron transfer from the conduction band of TiO_2 into interface states of the metal-organic framework/TiO_2 system.[54] Recovery takes place on a time scale of several nanoseconds (Figure 4e) as can be seen by the TA spectrum not changing after two nanoseconds. The absence of any evolution related to photoexcited TiO_2 shows that **1**-TiO_2 can effectively shutter the electron–hole recombination.

Based on the above results, we illustrate the mechanism for photocatalytic H_2 production by the cluster/semiconductor composite through a HOMO to LUMO + 1 transition as an example. Other main transitions under illumination with light are summarized in Table S1. The vacuum energy in absolute values is converted into redox potential with reference to the normal hydrogen electrode (NHE).[56] As illustrated in Figure 4c, only clusters are excited under visible light. The electrons in the HOMO of the clusters are excited to the LUMO + 1. As the energy level of LUMO + 1 is higher than that of the CB, the photoinduced electrons are spontaneously injected into the TiO_2 for H_2 production. The holes stay on the clusters for oxidation reactions. In this case, the clusters only serve as a photosensitizer, similar to a dye.[18] The charge-transfer channel switches when the light source changes. Under irradiation with UV/Vis light, both the cluster and semiconductor are excited, thereby generating electron–hole pairs (Figure 4f). With the driving force from the internal electric field, the holes in the VB of TiO_2 transfer to the HOMO of **1**, and electrons in **1** are injected into the CB of TiO_2, following a type II charge transfer pathway. The separation of photoinduced electron–hole pairs is more efficient in the type II photosystem. Thus, it enables more electrons to reduce protons adsorbed on the photocatalyst. In addition to the photosensitizer, the cluster also serves as co-catalyst in this case to facilitate charge separation.

The proposed mechanism for the cluster/semiconductor composite is different from the plasmonic metal nanoparticle/semiconductor system.[27] Schematic illustrations of the energy level diagram and the charge-transfer pathways in

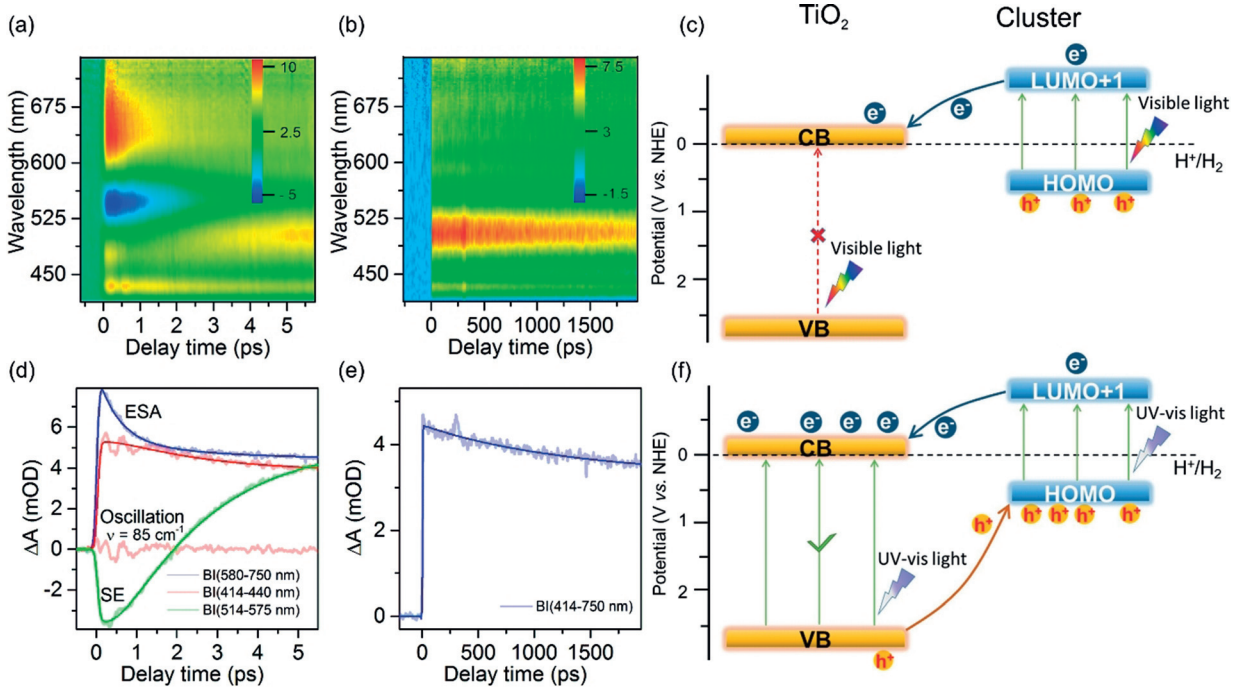

Figure 4. a,b) 2D pseudo-color plots of the transient absorption (TA) spectra of **1**-TiO_2 over different time scales. d,e) Summary of the kinetics of the TA. Early relaxation ($\tau = 0.7$ ps) is accompanied by an oscillation ($\nu = 85$ cm^{-1}). Decay of SE over 2.4 ps might indicate electron transfer from TiO_2 towards interface states. The hole–pair recombination of ca. 100 ps is suppressed in **1**-TiO_2 and the lifetime exceeds 2 ns. c,f) Schematic illustration of the charge-transfer pathways in the **1**-TiO_2 photocatalytic system for H_2 evolution. c) Under irradiation with visible light, only the clusters are excited. f) Under irradiation with UV/Vis light, both components are excited.

a typical TiO_2 system modified with Ag NPs are given in Figure S15 for comparison. The better charge separation efficiency of **1**-TiO_2(p), together with the good photosensitization ability of **1**, account for the better performance of **1**-TiO_2(p) than Ag NP-TiO_2 in the photocatalytic H_2 generation reaction (Figures 2b and S16).

In summary, a type II photosystem was built by the combination of TiO_2 with atomically precise silver NCs. The photocatalytic rate of H_2 generation by the composite is 7.4 mmol h^{-1} $g_{catalyst}^{-1}$, which is ten times higher than that of pristine TiO_2 NPs under the same conditions. The significantly enhanced performance is attributed to both the extension of the photoresponse and the efficient separation and transport of charge carriers. The role of the NCs as a small-band-gap semiconductor was revealed by the different charge-transfer routes occurring in the composite under different irradiation conditions. Under irradiation with visible light, the NCs only serve as a light-absorber. Under irradiation with UV/Vis light, the NCs also act as a small-band-gap semiconductor to improve the charge-separation efficiency. This type II photosystem endows the NCs with the ability to function as co-catalysts rather than merely photosensitizers. We believe that this study will stimulate more studies on using catalytically active metal NCs for the absorption of light and conversion of energy into relevant chemical fuels.

Acknowledgements

Y.W. thanks the Alexander von Humboldt Foundation, Bonn, Germany, for a postdoctoral fellowship and research grants. Q.C. thanks the support from the nature science foundation of China. (No. 21878242, No. 21828802). We thank Muhammad Hamid Raza and Jiao Wang for the ALD coating.

Conflict of interest

The authors declare no conflict of interest.

Keywords: charge transfer · co-catalysts · photosensitizers · silver nanoclusters

How to cite: *Angew. Chem. Int. Ed.* **2020**, *59*, 7748–7754
Angew. Chem. **2020**, *132*, 7822–7828

[1] R. Jin, C. Zeng, M. Zhou, Y. Chen, *Chem. Rev.* **2016**, *116*, 10346.
[2] I. Chakraborty, T. Pradeep, *Chem. Rev.* **2017**, *117*, 8208.
[3] M. A. Abbas, P. V. Kamat, J. H. Bang, *ACS Energy Lett.* **2018**, *3*, 840.
[4] A. W. Cook, T. W. Hayton, *Acc. Chem. Res.* **2018**, *51*, 2456.
[5] Q. Yao, T. Chen, X. Yuan, J. Xie, *Acc. Chem. Res.* **2018**, *51*, 1338.
[6] N. Sakai, T. Tatsuma, *Adv. Mater.* **2010**, *22*, 3185.
[7] C. Yu, G. Li, S. Kumar, H. Kawasaki, R. Jin, *J. Phys. Chem. Lett.* **2013**, *4*, 2847.
[8] H. Choi, Y.-S. Chen, K. G. Stamplecoskie, P. V. Kamat, *J. Phys. Chem. Lett.* **2015**, *6*, 217.
[9] M. A. Abbas, T.-Y. Kim, S. U. Lee, Y. S. Kang, J. H. Bang, *J. Am. Chem. Soc.* **2016**, *138*, 390.
[10] C. Azarias, C. Adamo, A. Perrier, *Phys. Chem. Chem. Phys.* **2016**, *18*, 7737.
[11] M. Pelton, Y. Tang, O. M. Bakr, F. Stellacci, *J. Am. Chem. Soc.* **2012**, *134*, 11856.
[12] S. H. Yau, O. Varnavski, T. Goodson, *Acc. Chem. Res.* **2013**, *46*, 1506.
[13] K. G. Stamplecoskie, P. V. Kamat, *J. Am. Chem. Soc.* **2014**, *136*, 11093.
[14] Y. Wang, X.-H. Liu, S. A. Kovalenko, Q.-Y. Chen, N. Pinna, *Chem. Eur. J.* **2019**, *25*, 4814.
[15] M. Zhou, T. Higaki, G. Hu, M. Y. Sfeir, Y. Chen, D.-E. Jiang, R. Jin, *Science* **2019**, *364*, 279.
[16] A. Kogo, N. Sakai, T. Tatsuma, *Nanoscale* **2012**, *4*, 4217.
[17] Y.-S. Chen, H. Choi, P. V. Kamat, *J. Am. Chem. Soc.* **2013**, *135*, 8822.
[18] Y.-S. Chen, P. V. Kamat, *J. Am. Chem. Soc.* **2014**, *136*, 6075.
[19] H. Wang, F. Chen, W. Li, T. Tian, *J. Power Sources* **2015**, *287*, 150.
[20] F. X. Xiao, S. F. Hung, J. Miao, H. Y. Wang, H. Yang, B. Liu, *Small* **2015**, *11*, 554.
[21] Y. Liu, Q. Yao, X. Wu, T. Chen, Y. Ma, C. N. Ong, J. Xie, *Nanoscale* **2016**, *8*, 10145.
[22] X. Cui, J. Wang, B. Liu, S. Ling, R. Long, Y. Xiong, *J. Am. Chem. Soc.* **2018**, *140*, 16514.
[23] F.-X. Xiao, Z. Zeng, B. Liu, *J. Am. Chem. Soc.* **2015**, *137*, 10735.
[24] Y. Gao, S. Bulusu, X. C. Zeng, *J. Am. Chem. Soc.* **2005**, *127*, 15680.
[25] R. Guo, R. W. Murray, *J. Am. Chem. Soc.* **2005**, *127*, 12140.
[26] L. Liao, S. Zhou, Y. Dai, L. Liu, C. Yao, C. Fu, J. Yang, Z. Wu, *J. Am. Chem. Soc.* **2015**, *137*, 9511.
[27] S. Linic, P. Christopher, D. B. Ingram, *Nat. Mater.* **2011**, *10*, 911.
[28] S. K. Cushing, J. Li, F. Meng, T. R. Senty, S. Suri, M. Zhi, M. Li, A. D. Bristow, N. Wu, *J. Am. Chem. Soc.* **2012**, *134*, 15033.
[29] H. Chen, X. E. Kou, Z. Yang, W. Ni, J. Wang, *Langmuir* **2008**, *24*, 5233.
[30] V. Subramanian, E. E. Wolf, P. V. Kamat, *J. Am. Chem. Soc.* **2004**, *126*, 4943.
[31] X.-H. Li, M. Antonietti, *Chem. Soc. Rev.* **2013**, *42*, 6593.
[32] D. Wang, Z. Liu, W. Yang, *ACS Catal.* **2018**, *8*, 7270.
[33] W.-N. Wang, W.-J. An, B. Ramalingam, S. Mukherjee, D. M. Niedzwiedzki, S. Gangopadhyay, P. Biswas, *J. Am. Chem. Soc.* **2012**, *134*, 11276.
[34] M. Sadeghi, W. Liu, T. G. Zhang, P. Stavropoulos, B. Levy, *J. Phys. Chem. C* **1996**, *100*, 19466.
[35] G. Li, R. Jin, *Acc. Chem. Res.* **2013**, *46*, 1749.
[36] S. Yamazoe, K. Koyasu, T. Tsukuda, *Acc. Chem. Res.* **2014**, *47*, 816.
[37] J. Yan, B. K. Teo, N. Zheng, *Acc. Chem. Res.* **2018**, *51*, 3084.
[38] K. Kwak, D. Lee, *Acc. Chem. Res.* **2019**, *52*, 12.
[39] Y. Wang, X.-K. Wan, L. T. Ren, H. F. Su, G. Li, S. Malola, S. C. Lin, Z. C. Tang, H. Häkkinen, B. K. Teo, Q. M. Wang, N. F. Zheng, *J. Am. Chem. Soc.* **2016**, *138*, 3278.
[40] H. Yang, Y. Wang, H. Huang, L. Gell, L. Lehtovaara, S. Malola, H. Häkkinen, N. Zheng, *Nat. Commun.* **2013**, *4*, 2422.
[41] Y. Negishi, K. Nobusada, T. Tsukuda, *J. Am. Chem. Soc.* **2005**, *127*, 5261.
[42] A. Desireddy, B. E. Conn, J. Guo, B. Yoon, R. N. Barnett, B. M. Monahan, K. Kirschbaum, W. P. Griffith, R. L. Whetten, U. Landman, T. P. Bigioni, *Nature* **2013**, *501*, 399.
[43] B. E. Conn, A. Atnagulov, B. Bhattarai, B. Yoon, U. Landman, T. P. Bigioni, *J. Phys. Chem. C* **2018**, *122*, 13166.
[44] T. Schultz, J. Niederhausen, R. Schlesinger, S. Sadofev, N. Koch, *J. Appl. Phys.* **2018**, *123*, 245501.
[45] H. Méndez, G. Heimel, S. Winkler, J. Frisch, A. Opitz, K. Sauer, B. Wegner, M. Oehzelt, C. Röthel, S. Duhm, D. Többens, N. Koch, I. Salzmann, *Nat. Commun.* **2015**, *6*, 8560.
[46] P. V. Kamat, J. Bisquert, *J. Phys. Chem. C* **2013**, *117*, 14873.
[47] S. Zhu, D. Wang, *Adv. Energy Mater.* **2017**, *7*, 1700841.
[48] K.-i. Ishibashi, A. Fujishima, T. Watanabe, K. Hashimoto, *Electrochem. Commun.* **2000**, *2*, 207.

[49] L. G. AbdulHalim, S. Ashraf, K. Katsiev, A. R. Kirmani, N. Kothalawala, D. H. Anjum, S. Abbas, A. Amassian, F. Stellacci, A. Dass, I. Hussain, O. M. Bakr, *J. Mater. Chem. A* **2013**, *1*, 10148.
[50] I. Chakraborty, W. Kurashige, K. Kanehira, L. Gell, H. Häkkinen, Y. Negishi, T. Pradeep, *J. Phys. Chem. Lett.* **2013**, *4*, 3351.
[51] Z. Chen, Q. Zhang, Y. Luo, *Angew. Chem. Int. Ed.* **2018**, *57*, 5320; *Angew. Chem.* **2018**, *130*, 5418.
[52] D. Shi, R. Zheng, M.-J. Sun, X. Cao, C.-X. Sun, C.-J. Cui, C.-S. Liu, J. Zhao, M. Du, *Angew. Chem. Int. Ed.* **2017**, *56*, 14637; *Angew. Chem.* **2017**, *129*, 14829.
[53] X.-H. Liu, F. Du, Q.-Y. Chen, Y.-H. Wang, *Electrochim. Acta* **2017**, *245*, 379.
[54] R. Li, J. Hu, M. Deng, H. Wang, X. Wang, Y. Hu, H.-L. Jiang, J. Jiang, Q. Zhang, Y. Xie, Y. Xiong, *Adv. Mater.* **2014**, *26*, 4783.
[55] P. Maioli, T. Stoll, H. E. Sauceda, I. Valencia, A. Demessence, F. Bertorelle, A. Crut, F. Vallée, I. L. Garzón, G. Cerullo, N. Del Fatti, *Nano Lett.* **2018**, *18*, 6842.
[56] C. Zoski, *Handbook of electrochemistry;* Elsevier, Amsterdam, **2007**.

Manuscript received: November 26, 2019
Revised manuscript received: February 2, 2020
Accepted manuscript online: February 18, 2020
Version of record online: March 18, 2020

